Smoothed-particle method for phase separation in polymer mixtures

Tohru Okuzono
Department of Physics, Ochanomizu University, Tokyo 112, Japan
(Received 10 July 1996; revised manuscript received 7 July 1997)

We propose a numerical model of the dynamics of phase separation in polymer mixtures based upon the generalized two-fluid model developed by Doi and Onuki [J. Phys. (France) II **2**, 1631 (1992)] using the method of smoothed-particle hydrodynamics. Our model is applicable to rheological studies of the phase-separating systems. We present our simulation results on the kinetics of domain growth and the phase separation under simple shear flow in two dimensions. We also discuss how the viscoelastic effect is incorporated into our model. [S1063-651X(97)06510-0]

PACS number(s): 61.25.Hq

I. INTRODUCTION

Polymer mixture is a typical fluid system where phase separation is observed. Many experimental observations [1] support the universal nature of the domain growth [2], that is, the algebraic growth law of the characteristic length and the dynamic scaling for the structure factor. Various numerical approaches have been made for this problem in the last decade [3–5]. Most of the numerical models are based upon the so-called model *H* of critical dynamics [6], or its variants which describe the dynamics of binary fluids. The cell dynamical system (CDS) method [7,8] provides an efficient way for the numerical simulations of the phase-separation phenomena, and extensive studies have been made using this method [3,4]. On the other hand, the molecular-dynamics method, which intrinsically involves hydrodynamics, has also been applied to the phase-separation phenomena [9,10]. However, since we are interested in the phase separation which occurs in macroscopic scales compared with a molecular scale, it is difficult to obtain reasonable results about the macroscopic-phase separation phenomena of complex fluids such as polymers by means of molecular-dynamics simulations.

In this paper we propose an alternative numerical model to describe the dynamics of phase separation in fluids based upon the generalized two-fluid model developed by Doi and Onuki [11], which reduces to the model *H* in some limit (see Sec. II). Our model is constructed based upon Lagrangian description of fluid rather than Eulerian one using the technique of smoothed-particle hydrodynamics (SPH) method [12]. In the SPH method ''fluid particles'' are sampled from the density field of fluid through a ''smoothing function.'' This procedure transforms the hydrodynamic partial differential equations into a set of ordinary differential equations, that is, equations of motion of particles. We apply this method to the two-fluid model. Thus the hydrodynamic effects are fully taken into account in our model.

It is interesting to study rheological properties of phase-separating systems where growing domains exist. Ohta, Nozaki, and Doi [13] performed computer simulations of phase separation under shear flow by means of the CDS method with no hydrodynamic interactions, and discussed the relation between rheological properties and domain morphology. A phenomenological study including the hydrodynamics was also done by Doi and Ohta [14]. Olson and Rothman [15] applied the lattice-gas model to this problem. Our model is also applicable to the rheology of phase-separating systems. In this paper we demonstrate simulations under simple shear flow in a two-dimensional system.

In the present study we ignore the viscoelastic effect due to the existence of the network stress of polymer chains. This effect will become important in dynamically asymmetric systems such as polymer solutions [16]. We discuss how to incorporate the viscoelastic effect into our model in Sec. IV. It should be emphasized that our approach does not restrict a problem to dynamics of polymer systems, but can be applied to general binary fluid systems. In the present study, specific features of polymer systems are taken into account only through the transport coefficients, and the Ginzburg-Landau free energy is used rather than the Flory-Huggins free energy. This may be justified at a temperature close to the critical point.

This paper is organized as follows. In Sec. II we briefly review the two-fluid model, and construct our numerical model in the absence of the elastic force. In Sec. III we carry out computer simulations. First, the domain growth problem is studied in two dimensions. Next, our model is applied to the dynamics of phase separation under simple shear flow in two dimensions. In Sec. IV we summarize results obtained in this study, and discuss a possible model which takes into account the viscoelastic effect for polymer solution systems.

II. MODEL

A. Two-fluid model

The two-fluid model was introduced by several authors as a phenomenological model to describe the dynamics of polymer solutions [17–21]. Doi and Onuki [11] generalized it for mixtures of polymer melts consisting of two kinds of polymers with molecular weights M_A and M_B. Their model includes the case of polymer solutions in the limit $M_B \ll M_A$. This model allows us to describe the dynamics of a quenched system into the spinodal region, that is, the dynamics of phase separation. We give a brief review of this generalized two-fluid model below.

Consider a mixture of two different kinds of polymers A and B with degrees of polymerization N_A and N_B, respectively. The system is assumed to be isothermal. In the two-fluid model, the local mass density ρ_X and the local velocity $\mathbf{v}_X$ of polymers, where $X=A$ or B, obey the following hy-

drodynamic equations including friction force terms caused by the relative motion between A and B polymers:

$$\frac{\partial \rho_X}{\partial t} = -\nabla\cdot(\rho_X \mathbf{v}_X), \tag{1}$$

$$\rho_X \frac{D\mathbf{v}_X}{Dt} = \phi_X \nabla\cdot\boldsymbol{\sigma}_X - \zeta(\mathbf{v}_X - \mathbf{v}_Y) + \mathbf{F}_X, \tag{2}$$

where the variables with indices X and Y are for the A and B polymers; the time derivative D/Dt is defined as $(\partial/\partial t)+\mathbf{v}_X\cdot\nabla$; ϕ_X is the local volume fraction of polymers X which is assumed to be equal to the mass fraction, that is, $\phi_X=\rho_X/\rho$, where $\rho=\rho_A+\rho_B$ is the total density; $\boldsymbol{\sigma}_X$ is the stress tensor; ζ is the friction coefficient which generally depends on ϕ_X; $\mathbf{F}_X$ is the extra force due to polymer networks. The stress tensor $\boldsymbol{\sigma}_X$ consists of the chemical potential and the viscous stress tensor

$$\boldsymbol{\sigma}_X = -(p+\mu_X)\mathbf{1} + \eta[(\nabla\mathbf{v})+(\nabla\mathbf{v})^T], \tag{3}$$

where μ_X is the chemical potential given by the relation $\mu_X=\delta F/\delta\phi_X$ with the total free energy F, $\mathbf{1}$ is the unit tensor, η is the shear viscosity, $\mathbf{v}\equiv\phi_A\mathbf{v}_A+\phi_B\mathbf{v}_B$ is the local average velocity of the total fluid, $(\nabla\mathbf{v})$ and $(\nabla\mathbf{v})^T$ are the velocity gradient tensor and its transpose, respectively, and p is the pressure which ensures the incompressibility condition $\nabla\cdot\mathbf{v}=0$ for the total fluid. The friction coefficient ζ is given by [11]

$$\zeta = \frac{\zeta_A\zeta_B}{\zeta_A+\zeta_B}, \tag{4}$$

with

$$\zeta_X = \phi_X \frac{N_X}{N_e}\zeta_{0X} \quad (X=A,B), \tag{5}$$

where N_e is the degree of polymerization between entanglement points, and ζ_{0X} is the microscopic friction constant of polymer X. The extra force $\mathbf{F}_X$ is related to the network stress $\boldsymbol{\sigma}^{(n)}$ which originates from the conformational entropy of polymer chains,

$$\mathbf{F}_X = \frac{\zeta_X}{\zeta_A+\zeta_B}\nabla\cdot\boldsymbol{\sigma}^{(n)}. \tag{6}$$

The stress tensor $\sigma^{(n)}$ generally depends on the past history of the deformation. For a polymer solution, for example, $\sigma^{(n)}$ would satisfy the following equation if the deformation is spatially homogeneous,

$$\sigma^{(n)} = \int_{-\infty}^{t} dt' G(t-t')\kappa(t') \tag{7}$$

where $G(t)$ is the stress relaxation function in the linear viscoelastic regime, and $\kappa(t)$ is the traceless part of the symmetric velocity gradient tensor for the polymers at time t, that is, $\kappa(t)\equiv(\nabla\mathbf{v}_A)+(\nabla\mathbf{v}_A)^T-\frac{2}{3}(\nabla\cdot\mathbf{v}_A)\mathbf{1}$ in three-dimensional space. (Hereafter we use the suffixes A and B for polymers and solvent in the polymer solution systems, respectively.) In the case of polymer mixtures, local velocity $\mathbf{v}_A$ in Eq. (7) should be replaced by the tube velocity introduced by Brochard [17], which is given by a linear combination of $\mathbf{v}_A$ and $\mathbf{v}_B$. Equations (1)–(7) give a closed set of equations for $\{\phi_X\}$ and $\{\mathbf{v}_X\}$ if the relaxation function $G(t)$ or an appropriate constitutive equation are given.

When the relative velocity $\mathbf{v}_A-\mathbf{v}_B$ is small compared with the average velocity $\mathbf{v}$ and its time derivative is negligible, Eqs. (1) and (2) are reduced to the hydrodynamic equation for $\mathbf{v}$ and the diffusion equation for ϕ_A (or ϕ_B),

$$\rho\frac{D\mathbf{v}}{Dt} = -(\phi_A-\phi_B)\nabla\frac{\delta F}{\delta\phi_A} + \nabla\cdot[\boldsymbol{\Pi}+\sigma^{(n)}], \tag{8}$$

$$\frac{\partial\phi_A}{\partial t} = -\nabla\cdot(\phi_A\mathbf{v}) + \nabla\left(\frac{2}{\zeta}\phi_A^2\phi_B^2\right)\cdot\left[\nabla\frac{\delta F}{\delta\phi_A} - g\nabla\cdot\boldsymbol{\sigma}^{(n)}\right], \tag{9}$$

where $\boldsymbol{\Pi}\equiv -p\mathbf{1}+\eta[(\nabla\mathbf{v})+(\nabla\mathbf{v})^T]$, and g is the coupling constant between diffusion and elastic stress which is given by

$$g = \frac{1}{\zeta_A+\zeta_B}\left(\frac{\zeta_A}{\phi_A}-\frac{\zeta_B}{\phi_B}\right). \tag{10}$$

If $N_A=N_B$ and $\zeta_{0A}=\zeta_{0B}$, then g vanishes. In such a case, we can expect that the elastic stress plays no important roles. Note that Eqs. (8) and (9) do not give a complete set of equations for $\mathbf{v}$ and ϕ_A because $\sigma^{(n)}$ generally depends on $\mathbf{v}_A$ and $\mathbf{v}_B$, and cannot be expressed in terms of $\mathbf{v}$ and ϕ_A. In the absence of $\sigma^{(n)}$ these equations are almost the same equations of the dynamical model for a critical binary fluid, the so-called model H [6], which has extensively been studied by many researchers, as mentioned in Sec. I.

B. Numerical model

There are many numerical methods to solve the hydrodynamic equations (1), (2), and (7). Here we adopt the Lagrangian description of fluid dynamics rather than a Eulerian description to construct a model. One of numerical methods based on the Lagrangian description is known as SPH [12] or smoothed-particle applied mechanics [22]. This method was used for some problems in astrophysics [12]. Recently, Posch, Hoover, and Kum [23] discussed a connection with molecular dynamics, and applied to the transport problem in Rayleigh-Bénard convection. The Lagrangian description is also useful for some simulations of flows in viscoelastic materials [24,25].

In the SPH method the smoothed density $\rho_s(\mathbf{r})$ of the mass density $\rho(\mathbf{r})$ of fluid at position $\mathbf{r}$ plays a fundamental role. $\rho_s(\mathbf{r})$ is defined by using a smoothing function $W(\mathbf{r},h)$,

$$\rho_s(\mathbf{r}) = \int W(\mathbf{r}-\mathbf{r}',h)\rho(\mathbf{r}')d\mathbf{r}'. \tag{11}$$

The kernel $W(\mathbf{r},h)$ has the following properties [12]:

$$\int W(\mathbf{r},h)d\mathbf{r}=1, \quad \lim_{h\to 0} W(\mathbf{r},h)=\delta(\mathbf{r}). \tag{12}$$

The parameter h defines the smoothing length of the kernel $W(\mathbf{r},h)$. A typical example of $W(\mathbf{r},h)$ is the Gaussian kernel, that is,

$$W(\mathbf{r},h)=\frac{1}{(\pi h^2)^{d/2}}e^{-\mathbf{r}^2/h^2}, \tag{13}$$

where d is the spatial dimension. This smoothing function defines a fluid element or a fluid particle with size h. If we choose a set of random points $\mathbf{r}_1,\mathbf{r}_2,\ldots,\mathbf{r}_N$ with a probability density which is proportional to $\rho(\mathbf{r})$, we can evaluate the integral in Eq. (11) with the Monte Carlo integration method,

$$\rho_s(\mathbf{r})\simeq\sum_{j=1}^{N} mW(\mathbf{r}-\mathbf{r}_j,h), \tag{14}$$

where $m\equiv(1/N)\int\rho(\mathbf{r})d\mathbf{r}$, and N is the total number of sampling points. These sampling points are regarded as positions of fluid particles having mass m and size h. The physical quantities (mass, momentum, and energy) of the fluid are transported by the motion of particles in the SPH. It may be reasonable to choose the correlation length of density fluctuations as the particle size h. The density at the position of particle i is given by $\rho_i\equiv\rho_s(\mathbf{r}_i)$. For a given field $A(\mathbf{r})$, its smoothed field $A_s(\mathbf{r})$ is given by

$$A_s(\mathbf{r})\simeq\sum_{j=1}^{N} m\frac{A(\mathbf{r}_j)}{\rho_j}W(\mathbf{r}-\mathbf{r}_j,h). \tag{15}$$

With these expressions of field quantities, we can derive a set of equations of motion of the fluid particles from the hydrodynamic partial differential equations. Note that the smoothed density given by Eq. (14) is differentiable, and the gradient of density, for example, is expressed as a superposition of gradients of the kernel $\nabla W(\mathbf{r}-\mathbf{r}_j,h)$. For detailed procedures of deriving equations of motion of the particles, see Ref. [12].

Based upon the above picture of the fluid particles, we construct a model for polymer mixtures which will provide an alternative expression of the two-fluid model described in Sec. II A. Of course we can directly derive equations of motion from Eqs. (1) and (2) through the formal procedure of SPH method. Here, however, we derive the equations of motion in some heuristic manner. Let us consider two kinds of particles A and B whose positions are $\{\mathbf{r}_i\}$ $(i=1,2,\ldots,\mathcal{N}_A)$ and $\{\mathbf{r}_m\}$ $(m=1,2,\ldots,\mathcal{N}_B)$, respectively, where $\mathcal{N}_A$ and $\mathcal{N}_B$ are the total number of A and B particles, respectively. Hereafter we use the indices $i,j,\ldots$ and $m,n,\ldots$ for A and B particles, respectively, and $\alpha,\beta,\ldots$ for any particles. The densities $\rho_A(\mathbf{r})$ and $\rho_B(\mathbf{r})$ of the A and B fluids, respectively, are given by

$$\rho_A(\mathbf{r})=\sum_{j=1}^{\mathcal{N}_A} m_AW(\mathbf{r}-\mathbf{r}_j,h),\quad \rho_B(\mathbf{r})=\sum_{n=1}^{\mathcal{N}_B} m_BW(\mathbf{r}-\mathbf{r}_n,h), \tag{16}$$

where $m_A\equiv\mathcal{M}_A/\mathcal{N}_A$ and $m_B\equiv\mathcal{M}_B/\mathcal{N}_B$, with the total mass $\mathcal{M}_A$ and $\mathcal{M}_B$ of the A and B fluids in the whole system, respectively. The total density is given by $\rho(\mathbf{r})=\rho_A(\mathbf{r})+\rho_B(\mathbf{r})$. It must be noted that in our model the strict incompressible flow cannot be realized, and here we consider a *nearly incompressible* fluid. Therefore, small spatial variations of $\rho(\mathbf{r})$ should be allowed. We define the local velocities of the A and B fluids, $\mathbf{v}_A(\mathbf{r})$ and $\mathbf{v}_B(\mathbf{r})$, respectively, as

$$\mathbf{v}_A(\mathbf{r})=\sum_j \frac{m_A}{\rho_{Aj}}\dot{\mathbf{r}}_jW(\mathbf{r}-\mathbf{r}_j,h),$$

$$\mathbf{v}_B(\mathbf{r})=\sum_n \frac{m_B}{\rho_{Bn}}\dot{\mathbf{r}}_nW(\mathbf{r}-\mathbf{r}_n,h), \tag{17}$$

where $\rho_{Aj}\equiv\rho_A(\mathbf{r}_j)$, $\rho_{Bn}\equiv\rho_B(\mathbf{r}_n)$, and $\dot{\mathbf{r}}_\alpha\equiv(d/dt)\mathbf{r}_\alpha$ is the velocity of particle α. We also define the average velocity $\mathbf{v}(\mathbf{r})$,

$$\mathbf{v}(\mathbf{r})=\sum_\beta \frac{m_\beta}{\rho_\beta}\dot{\mathbf{r}}_\beta W(\mathbf{r}-\mathbf{r}_\beta,h), \tag{18}$$

where $m_\beta=m_A$ or m_B for particle β of type A or B, respectively, and $\rho_\beta\equiv\rho(\mathbf{r}_\beta)$.

To derive the equations of motion of particles, we construct a Lagrangian and a dissipation function in terms of the variables related to the particles. Although the elastic energy which causes the extra force in Eq. (2) plays a crucial role in dynamically asymmetric systems [16] such as polymer solutions, here we consider, as a first step, a system in which the elastic force dose not play any significant role. Such a system is a polymer blend where the coupling constant g in Eq. (10) vanishes as mentioned in Sec. II A. We have also assumed that the system is isothermal. Thus we write the Lagrangian $\mathcal{L}$ in the form

$$\mathcal{L}=\sum_\beta m_\beta\left[\frac{1}{2}\dot{\mathbf{r}}_\beta^2-f(\rho_\beta,\phi_{A\beta},\phi_{B\beta})\right], \tag{19}$$

where $f(\rho_\beta,\phi_{A\beta},\phi_{B\beta})$ is the thermodynamic potential or free energy per unit mass and $\phi_{A\beta}\equiv\rho_{A\beta}/\rho_\beta$ and $\phi_{B\beta}\equiv\rho_{B\beta}/\rho_\beta$ are the mass fractions of the A and B fluids, respectively.

Since we are considering a nearly incompressible fluid, we ignore the bulk viscosity of the total fluid. In this case, the dissipation arises from shearing motion of the fluid and the ''friction'' between the two fluids, which is a feature of the two-fluid model. Hence the dissipation function $\mathcal{R}$ is given by

$$\mathcal{R}=\sum_\beta \frac{m_\beta}{\rho_\beta}\eta\mathbf{D}_\beta:\mathbf{D}_\beta+\frac{1}{2}\sum_\beta \frac{m_\beta}{\rho_\beta}\zeta_\beta(\mathbf{v}_A-\mathbf{v}_B)_\beta^2, \tag{20}$$

where $\mathbf{D}_\beta$ is the traceless part of symmetric velocity gradient tensor $\frac{1}{2}[(\nabla\mathbf{v})_\beta+(\nabla\mathbf{v})_\beta^T]$, $\zeta_\beta\equiv\zeta(\phi_\beta)$, and $(\cdots)_\beta$ denotes an estimation of a field quantity at $\mathbf{r}_\beta$. Here we have assumed that both the two polymer melts A and B have the same viscosity η. The velocity gradient tensor and the difference of velocities between A and B fluids are written, in the particle system, as

$$(\nabla\mathbf{v})_\alpha=\sum_\beta \frac{m_\beta}{\rho_\alpha}(\dot{\mathbf{r}}_\beta-\dot{\mathbf{r}}_\alpha)\nabla_\alpha W_{\alpha\beta}, \tag{21}$$

$$(\mathbf{v}_A-\mathbf{v}_B)_\alpha=\sum_j \frac{m_A}{\rho_{Aj}}\dot{\mathbf{r}}_j W_{\alpha j}-\sum_n \frac{m_B}{\rho_{Bn}}\dot{\mathbf{r}}_n W_{\alpha n}, \tag{22}$$

where $W_{\alpha\beta}\equiv W(\mathbf{r}_\alpha-\mathbf{r}_\beta,h)$ and $\nabla_\alpha W_{\alpha\beta}\equiv(\partial/\partial\mathbf{r}_\alpha)W_{\alpha\beta}$. Note that $\nabla_\alpha W_{\alpha\beta}$ is given by $-2(\mathbf{r}_\alpha-\mathbf{r}_\beta)W_{\alpha\beta}/h^2$ for the Gaussian kernel $W_{\alpha\beta}$. In actual simulations, ρ_α in Eq. (21) is replaced by $\rho_{\alpha\beta}\equiv\frac{1}{2}(\rho_\alpha+\rho_\beta)$ for a symmetrical reason [12,22].

From Eqs. (19) and (20), we can derive the equation of motion of particle α in the form of the usual Euler-Lagrange equation in the presence of dissipation,

$$\frac{d}{dt}\frac{\partial\mathcal{L}}{\partial\dot{\mathbf{r}}_\alpha}-\frac{\partial\mathcal{L}}{\partial\mathbf{r}_\alpha}+\frac{\partial\mathcal{R}}{\partial\dot{\mathbf{r}}_\alpha}=0. \tag{23}$$

The first term in Eq. (23) yields the acceleration term $m_\alpha\ddot{\mathbf{r}}_\alpha$, where $\ddot{\mathbf{r}}_\alpha\equiv(d^2/dt^2)\mathbf{r}_\alpha$. The second one is a potential force that may be written by

$$-\frac{\partial\mathcal{L}}{\partial\mathbf{r}_\alpha}=\sum_\beta m_\beta\left[\left(\frac{\partial f}{\partial\rho}\right)_\beta\frac{\partial\rho_\beta}{\partial\mathbf{r}_\alpha}+\left(\frac{\partial f}{\partial\phi_A}-\frac{\partial f}{\partial\phi_B}\right)_\beta\frac{\partial\phi_{A\beta}}{\partial\mathbf{r}_\alpha}\right], \tag{24}$$

where the condition $\phi_A+\phi_B=1$ is used. Noting that $(\partial f/\partial\rho)_\beta=p_\beta/\rho_\beta^2$, from Eqs. (16) and (24) we obtain

$$-\frac{\partial\mathcal{L}}{\partial\mathbf{r}_\alpha}=\sum_\beta m_\alpha m_\beta\left(\frac{p_\alpha+\mu_{\alpha\beta}}{\rho_\alpha^2}+\frac{p_\beta+\mu_{\beta\alpha}}{\rho_\beta^2}\right)\nabla_\alpha W_{\alpha\beta}, \tag{25}$$

where $\mu_{\alpha\beta}\equiv\mu_\alpha$ or $-\mu_\alpha$ for particle β of type A or B, respectively, and μ_α is the chemical potential per unit volume of particle α defined by

$$\mu_\alpha\equiv\frac{1}{2}\rho_\alpha\left[\left(\frac{\partial f}{\partial\phi_A}\right)_\alpha-\left(\frac{\partial f}{\partial\phi_B}\right)_\alpha\right], \tag{26}$$

and p_α is an estimation of the pressure field $p(\mathbf{r})$ for the total fluid at the point $\mathbf{r}=\mathbf{r}_\alpha$. In the two-fluid model the pressure p is determined to keep the incompressibility $\nabla\cdot\mathbf{v}=0$. In our scheme, however, the strict incompressibility cannot be satisfied, and we regard the pressure as a penalty for the incompressibility. Adiabatic approximations using Poisson's relation $p\propto\rho^\gamma$ with specific heat ratio γ are often used in SPH simulations for compressible flow. Here we use the similar expression for the pressure. We choose the following simple form for the pressure, or penalty, function:

$$p_\alpha=p_0\left[\left(\frac{\rho_\alpha}{\overline{\rho}}\right)^2-1\right], \tag{27}$$

where p_0 is a positive constant and $\overline{\rho}$ is the average mass density. For the physical argument about possible form of equation of state, see Ref. [22].

Now we extend the model to incorporate the effect of spatial inhomogeneity of ϕ_A or ϕ_B. We assume that the chemical potential is derived from an appropriate free energy functional F such as Flory–Huggins–de Gennes free energy [18]. Although asymmetry of the free-energy potential is important for the systems of polymer solutions [16], here we use the symmetric Ginzburg-Landau-type free energy, which leads to

$$\mu_\alpha=-\epsilon S_\alpha+uS_\alpha^3-K(\nabla^2S)_\alpha, \tag{28}$$

where $S\equiv\phi_A-\phi_B$ is the order parameter and S_α is that evaluated at $\mathbf{r}_\alpha$, ϵ is the quench depth, and u and K are positive constants. Since we are considering nearly incompressible fluids, we use the approximation $(\nabla^2S)_i\simeq2(\nabla^2\rho_A)_i/\rho_i$ and the following expression for the Laplacian:

$$(\nabla^2\rho_A)_i=\sum_j\frac{m_A}{\rho_{Ai}}[(\nabla\rho_A)_j-(\nabla\rho_A)_i]\cdot\nabla_i W_{ij}, \tag{29}$$

with

$$(\nabla\rho_A)_i=\sum_j m_A\nabla_i W_{ij}, \tag{30}$$

where the identity $\rho_A\nabla^2\rho_A=\nabla\cdot(\rho_A\nabla\rho_A)-(\nabla\rho_A)^2$ is used. In Eq. (29) ρ_{Ai} is replaced by $\rho_{Aij}\equiv\frac{1}{2}(\rho_{Ai}+\rho_{Aj})$ in actual simulations for the same reason as before. For numerical calculations, it is convenient to use the variables $c_\alpha\equiv\rho_{A\alpha}$ or $\rho_{B\alpha}$ for particle α of type A or B, respectively, and $\hat{S}_\alpha\equiv2c_\alpha/\rho_\alpha-1$. Using these variables, $\mu_{\alpha\beta}$ appeared in Eq. (25) which represents the potential interaction between particles α and β written by

$$\mu_{\alpha\beta}=\epsilon_{\alpha\beta}\hat{\mu}_\alpha, \tag{31}$$

where $\hat{\mu}_\alpha\equiv-\epsilon\hat{S}_\alpha+u\hat{S}_\alpha^3-K(\nabla^2\hat{S})_\alpha$, and $\epsilon_{\alpha\beta}$ takes 1 or -1 according whether particles α and β are the same type or not, respectively. As one can see from Eqs. (25) and (28) or (31), the interaction forces between particles depend on the densities or the order parameters at their points. That is a different point from usual molecular-dynamics simulations.

Calculations of the last term in Eq. (23) are straightforward. Making use of the properties $W_{\alpha\beta}=W_{\beta\alpha}$ and $\nabla_\alpha W_{\alpha\beta}=-\nabla_\beta W_{\beta\alpha}$, we finally obtain the following equations of motion of particles:

$$\ddot{\mathbf{r}}_\alpha=\sum_\beta m_\beta\left(\frac{\boldsymbol{\sigma}_{\alpha\beta}}{\rho_\alpha^2}+\frac{\boldsymbol{\sigma}_{\beta\alpha}}{\rho_\beta^2}\right)\cdot\nabla_\alpha W_{\alpha\beta}$$

$$\mp\sum_\beta\frac{m_\beta}{\rho_\beta c_\alpha}\zeta_\beta(\mathbf{v}_A-\mathbf{v}_B)_\beta W_{\beta\alpha}, \tag{32}$$

where we take the minus (plus) sign in front of the last term in Eq. (32) for particle α of type A (B), and the tensor $\boldsymbol{\sigma}_{\alpha\beta}$ is defined by

$$\boldsymbol{\sigma}_{\alpha\beta}\equiv-(p_\alpha+\mu_{\alpha\beta})\mathbf{1}+2\eta\mathbf{D}_\alpha. \tag{33}$$

This tensor $\boldsymbol{\sigma}_{\alpha\beta}$ is associated with the interaction between particle α and β. The index $\alpha\beta$ does not mean the tensor component. Equation (32) corresponds to Eq. (2) in the absence of $\mathbf{F}_\alpha$ and the continuity equation (1) is automatically satisfied in our model. The last term in Eqs. (32) can be simplified as

$$\sum_{\beta} \frac{m_\beta}{\rho_\beta c_\alpha} \zeta_\beta (\mathbf{v}_A - \mathbf{v}_B)_\beta W_{\beta\alpha} \simeq \frac{\zeta_\alpha}{c_\alpha} (\mathbf{v}_A - \mathbf{v}_B)_\alpha \tag{34}$$

if the friction force $\zeta_\beta(\mathbf{v}_A-\mathbf{v}_B)_\beta$ and the density ρ_β do not largely change in space. We use this expression in the following simulations.

Note that our model is also applicable to low-molecular binary fluids if we set the friction coefficient ζ_α to be constant. A feature of polymeric systems presents only in the dependence of ζ_α on ϕ_α in our model.

III. SIMULATIONS AND RESULTS

In order to carry out numerical simulations we must write the equations of motion in dimensionless form. In this section all physical quantities are scaled by using l_0, u_0, and ρ_0 which are units of length, velocity, and mass density, respectively, and we use the same notations of the dimensionless variables as their corresponding dimensionful variables. If we scale the energy density by $\rho_0 u_0^2$, equations of motion (32) now become

$$\ddot{\mathbf{r}}_\alpha = \sum_\beta m_\beta \left(\frac{\boldsymbol{\sigma}_{\alpha\beta}}{\rho_\alpha^2} + \frac{\boldsymbol{\sigma}_{\beta\alpha}}{\rho_\beta^2} \right) \cdot \nabla_\alpha W_{\alpha\beta} \mp \mathfrak{P} \frac{\zeta_\alpha}{c_\alpha} (\mathbf{v}_A - \mathbf{v}_B)_\alpha , \tag{35}$$

with the dimensionless tensor

$$\sigma_{\alpha\beta} = -(p_\alpha + \mu_{\alpha\beta})\mathbf{1} + 2\mathfrak{R}^{-1}\mathbf{D}_\alpha . \tag{36}$$

where approximation (34) has been used. $\mathfrak{R}$ and $\mathfrak{P}$ in Eqs. (35) and (36) are the dimensionless parameters defined as

$$\mathfrak{R} \equiv \frac{\rho_0 u_0 l_0}{\eta}, \quad \mathfrak{P} \equiv \frac{\tilde{\zeta}_0 l_0}{\rho_0 u_0}, \tag{37}$$

where $\tilde{\zeta}_0 \equiv \zeta_0 N/N_e$, and $\zeta_{0A} = \zeta_{0B} \equiv \zeta_0$ has been assumed, so that ζ_α in Eq. (35) is given by $(\phi_A \phi_B)_\alpha$. Our system is controlled by these two parameters. $\mathfrak{R}$ and $\mathfrak{P}^{-1}$ represent strength of inertia and diffusion of the order parameter, respectively. Since $\tilde{\zeta}_0$ is estimated as $\tilde{\zeta}_0 \sim L^{-1}$, where L is the kinetic coefficient of polymers, ratio of the strength of the above two effects is estimated as

$$\mathfrak{R}\mathfrak{P} \sim \frac{l_0^2}{\eta L} \sim \left(\frac{l_0}{R_G} \right)^2 \frac{N_e}{N}, \tag{38}$$

where R_G is the gyration radius of a polymer chain. Here we have used the following estimation, $\eta L \sim R_G^2 N/N_e$ in the reptation dynamics [13,26]. It should be noted that η should be regarded as the viscosity of polymer melts (the same viscosity of the both A and B polymers are assumed), since we are here considering the polymer blend. In the Rouse dynamics the factor N_e/N in Eq. (38) is of order unity. Hence $\mathfrak{R}\mathfrak{P} \sim (l_0/R_G)^2 \sim 1$ if we choose $l_0 \sim R_G$. In this study we consider the above situation. The chemical potential is assumed to be given by

$$\mu_\alpha = -\epsilon S_\alpha + S_\alpha^3 - \hat{K}(\nabla^2 S)_\alpha , \tag{39}$$

and both $\hat{K}$ and $|\epsilon|$ are fixed at 0.5 in the present study.

Other parameters are determined as follows. We use the Gaussian kernel W given by Eq. (13). The particle size h is determined as $h = (V/\mathcal{N})^{1/d} = 1$, where V is the total volume of the system, and we set $\mathcal{N} \equiv \mathcal{N}_A = \mathcal{N}_B$. Note that the interface width, $\xi \equiv (\hat{K}/|\epsilon|)^{1/2}$, is unity in our system. The average mass density $\bar{\rho}$ is set to be unity. Hence the particle mass is given by $m_A = \Phi V/\mathcal{N}_A$, $m_B = (1-\Phi)V/\mathcal{N}_B$, where $\Phi \equiv \int \rho_A(\mathbf{r})d\mathbf{r} / \int \rho(\mathbf{r})d\mathbf{r}$ is the total mass (or volume) fraction of A fluid. The pressure p_α is now given by

$$p_\alpha = p_0(\rho_\alpha^2 - 1). \tag{40}$$

Recall that the pressure p_α does not mean there are two different pressure associated with A and B particles, but mean that p_α is the pressure at the point $\mathbf{r} = \mathbf{r}_\alpha$.

A. Domain growth kinetics

Now we numerically solve Eqs. (35)–(40) under the periodic boundary conditions. We carry out the simulation of a two-dimensional system with $\mathcal{N} = 10\,000$. The time integration is done by the fourth-order Runge-Kutta-Gill method with a time step $\Delta t = 0.1$. We have a cutoff length r_c for the interaction range between particles, and here we set $r_c = 3.0$. Initial configurations are created a the following way. We place A and B particles on a square lattice, and its dual lattice, respectively, and randomize their positions using the uniform random numbers with amplitude 0.5 (the lattice spacing is unity). The velocities of each particle are set to be zero. From this initial configuration we relax the system during 100 time steps with $\epsilon = -0.5$ to obtain a disordered state. After this initial relaxation process we quench, at $t = 0$, the system to $\epsilon = 0.5$. We set $p_0 = 2.0$ in Eq. (40) so that the nearly incompressible flow is realized. Indeed in the following simulations the total mass density ρ_α satisfies $0.95 < \rho_\alpha < 1.05$ for every particle α in any time except for the initial relaxation process.

After the quench the linearly unstable fluctuation modes rapidly grow, and domain structures emerge. This domain pattern coarsens in time and the system evolves toward an equilibrium two-phase coexistent state. Some snapshots of the time-evolving pattern with $\mathfrak{R}^{-1} = \mathfrak{P} = 1$ and $\Phi = 0.5$ are shown in Fig. 1. In these figures the mass density of A fluid is indicated by the gray scale, that is, bright or dark regions correspond to A- or B-rich regions of the fluid, respectively.

Now we define a structure factor $I(\mathbf{k},t)$ as a quantitative measure of the pattern evolution,

$$I(\mathbf{k},t) \equiv \langle \rho_A(\mathbf{k},t)\rho_A(-\mathbf{k},t)\rangle / \int d\mathbf{k} \langle \rho_A(\mathbf{k},t)\rho_A(-\mathbf{k},t)\rangle, \tag{41}$$

where $\rho_A(\mathbf{k},t)$ is the Fourier component of $\rho_A(\mathbf{r})$ with wave vector $\mathbf{k}$ at time t and $\langle \cdots \rangle$ denotes the ensemble average for initial configurations. Since $\rho_A(\mathbf{k},t) = \hat{\rho}_A(\mathbf{k}) W(\mathbf{k})$ from Eq. (16), where $W(\mathbf{k})$ and $\hat{\rho}_A(\mathbf{k})$ are the Fourier components of $W(\mathbf{r},h)$ and $\hat{\rho}_A(\mathbf{r}) \equiv \Sigma_j m_A \delta(\mathbf{r} - \mathbf{r}_j)$, respectively, $I(\mathbf{k},t)$ can be calculated by using the method [41] which is familiar in molecular dynamics simulations. However, we calculate it by using fast Fourier transformation after mapping $\rho_A(\mathbf{r})$

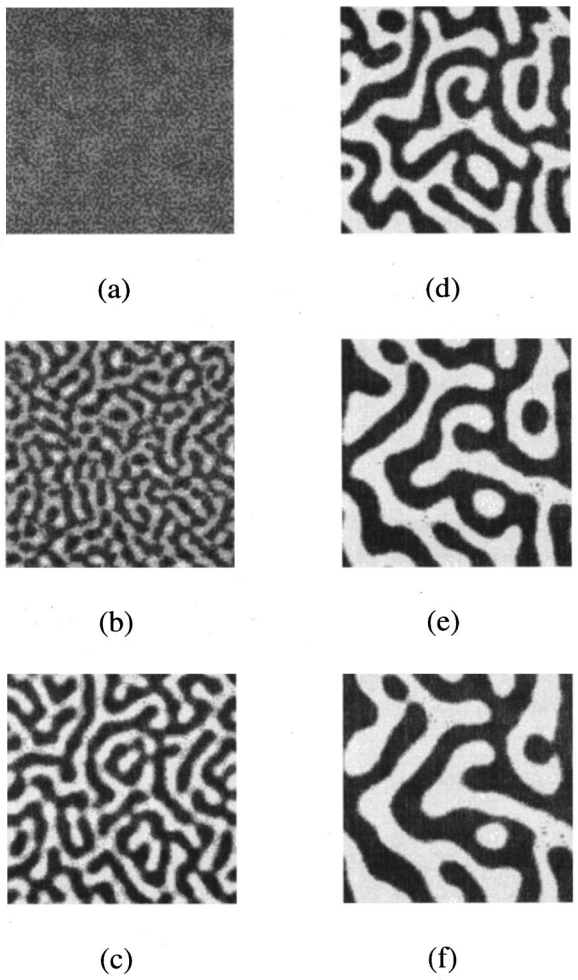

FIG. 1. Snapshots of the domain pattern at $t=0$ (a), 50 (b), 100 (c), 200 (d), 300 (e), and 400 (f). The mass density of the A fluid is shown by gray scales. Bright regions correspond to A-rich domains. $\mathfrak{R}^{-1}=\mathfrak{P}=1.0$ and $\Phi=0.5$.

given by Eq. (16) onto a square lattice because it takes less computation time. Here we use a 128^2 square lattice.

The first moment $k_1(t)$ of the circular averaged structure factor denoted by $I(k,t)$ ($k\equiv|\mathbf{k}|$) defines a characteristic wave number whose inverse gives the characteristic length $l(t)$. In Fig. 2, doubly logarithmic plots of $k_1(t)$ for some runs with different parameters are shown for the case $\Phi=0.5$. Squares, circles, triangles, and diamonds in this figure correspond to the runs for $\mathfrak{R}^{-1}=2.0$, 1.0, 0.7, and 0.5, respectively. $\mathfrak{P}$ is fixed at 1.0 for all runs. For $\mathfrak{R}^{-1}\geqslant 1.0$ we observe the growth law $k_1(t)\sim t^{-z}$ with $z\simeq\frac{1}{2}$ asymptotically (the solid line in Fig. 2 indicates the slope $-\frac{1}{2}$). The exponent z increases as $\mathfrak{R}^{-1}$ decreases. In particular, for $\mathfrak{R}^{-1}=0.5$, it seems that there is a crossover of the exponent from $z=\frac{1}{2}$ to $\frac{2}{3}$ (the dashed line indicates the slope $-\frac{2}{3}$).

It is believed that the characteristic length $l(t)$ of the domains linearly grows with time in the late stage, that is, $l(t)\sim t$, in three-dimensional binary fluid systems, without an inertia effect at critical quench where interconnected domains with sharp interfaces are formed [2,27,28,30]. However, Furukawa [30,31] predicted that the phase-separation dynamics in fluid systems in both two and three dimensions

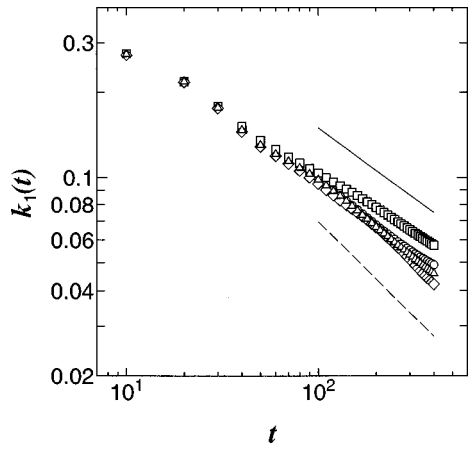

FIG. 2. Double-logarithmic plots of $k_1(t)$, the first moment of the structure factor $I(k,t)$. The symbols □, ○, △, and ◇ correspond to the runs with $\mathfrak{R}^{-1}=2.0$, 1.0, 0.7, and 0.5, respectively. $\mathfrak{P}$ is fixed at 1.0 and $\Phi=0.5$. Solid and dashed lines show the slopes $-\frac{1}{2}$ and $-\frac{2}{3}$, respectively.

is inevitably affected by the inertia effect in the long-time limit and $z=\frac{2}{3}$ in that regime, and that in two-dimensional systems there is a crossover from the Brownian coagulation regime ($z=\frac{1}{2}$) to the inertia-controlled regime ($z=\frac{2}{3}$). In fact, a $t^{2/3}$ growth law has been obtained by the lattice-gas model [32] in three dimensions, and several numerical studies in two-dimensional fluid systems have shown that $z=\frac{1}{2}-\frac{2}{3}$ [29,9,10]. Since the parameter $\mathfrak{R}^{-1}$ controls the inertia, our result agrees with Furukawa's prediction. However, the Brownian coagulation mechanism for $t^{1/2}$ growth law is not appropriate here because there is no thermal noise in our system.

Next we examine the dynamic scaling for the structure factor $I(k,t)$. We plot $k_1^2(t)I(k,t)$ versus $k/k_1(t)$ in Fig. 3 at $t=250$, 300, 350, and 400 with symbols ○, □, ◇, and △, respectively. These data are obtained by averaging over five independent runs with $\mathfrak{R}^{-1}=\mathfrak{P}=1.0$. This figure suggests the existence of the dynamic scaling function $F(x)\equiv k_1^2(t)I(k,t)$ with $x\equiv k/k_1(t)$. To see the behavior of $F(x)$ more precisely we show doubly logarithmic plots of

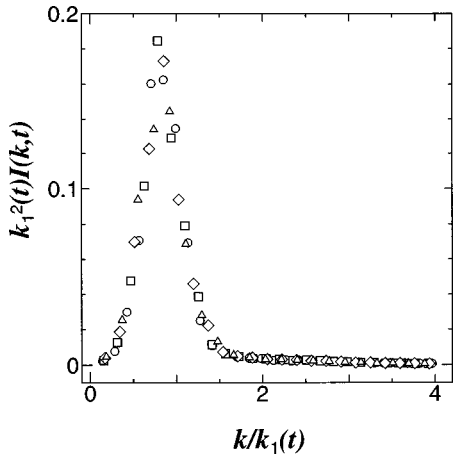

FIG. 3. Scaling plots of the structure factor $I(k,t)$ for $\mathfrak{R}^{-1}=\mathfrak{P}=1.0$ and $\Phi=0.5$. The symbols ○, □, ◇, and △ correspond to $t=250$, 300, 350, and 400, respectively.

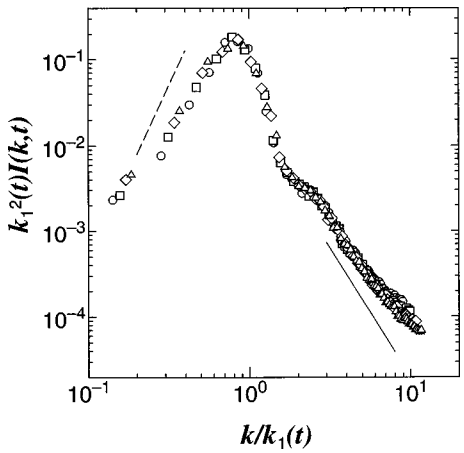

FIG. 4. Double-logarithmic plots of $F(x)$ after hardening transformation. The meanings of the symbols are the same as those in Fig. 3.

$F(x)$ in Fig. 4 (the meanings of the symbols are the same as those in Fig. 3). Here we have used the data obtained after ''hardening'' transformation [33] [$\rho_A(\mathbf{r})\rightarrow\theta(\rho_A(\mathbf{r})-\frac{1}{2})$, $\theta(\cdots)$ is the step function] to avoid the effect of finite thickness of interfaces. We see that $F(x)$ behaves like x^4 [34,35] for small x except for very small x, where the finite system size may have an effect, and there is a ''shoulder'' [36] at $x=2-3$. It appears that Porod's law [37] [$F(x)\sim x^{-(d+1)}$] holds for large x in the long time limit. Solid and dashed lines in Fig. 4 show the slopes -3 and 4, respectively. These features of $F(x)$ are commonly observed in other computer simulations [3,4] and experiments [38–40], although the present simulation is in two dimensions and we cannot directly compare with three-dimensional results.

In Fig. 5 we also show snapshots for the case of off-critical quench, $\Phi=0.4$, and $\mathfrak{R}^{-1}=\mathfrak{P}=1.0$. In this case the dropletlike pattern grows, and we observe a slower growth law with exponent $z\simeq\frac{1}{3}$ (Fig. 6). The droplet growth mainly occurs by the coalescence between droplets although we also observe the process of evaporation-condensation type. At this time, however, it is not clear which mechanism of the droplet growth is relevant to the growth law in Fig. 6.

B. Phase separation under shear flow

Our model can be applied to phase separation in the presence of shear flow by employing the technique of nonequilibrium molecular dynamics [41]. Here we use the so-called Sllod method [41] for simple shear in a two-dimensional system with the Lees-Edwards boundary conditions [41]. (The ''Sllod'' method is so named because of its close relationship to the Dolls tensor algorithm.) The equations of motion are now written by

$$\frac{d}{dt}r_{\alpha x}=\tilde{v}_{\alpha x}+r_{\alpha y}\dot{\gamma},\quad \frac{d}{dt}r_{\alpha y}=\tilde{v}_{\alpha y}, \tag{42}$$

$$\frac{d}{dt}\tilde{v}_{\alpha x}=f_{\alpha x}-\tilde{v}_{\alpha y}\dot{\gamma},\quad \frac{d}{dt}\tilde{v}_{\alpha y}=f_{\alpha y}, \tag{43}$$

where $r_{\alpha x}$ ($r_{\alpha y}$) and $\tilde{v}_{\alpha x}$ ($\tilde{v}_{\alpha y}$) are the x (y) component of position and deviation of velocity from uniform shear of particle α, respectively, $\mathbf{f}_\alpha\equiv(f_{\alpha x},f_{\alpha y})$ is the right-hand side of Eq. (35), and $\dot{\gamma}$ is the shear rate.

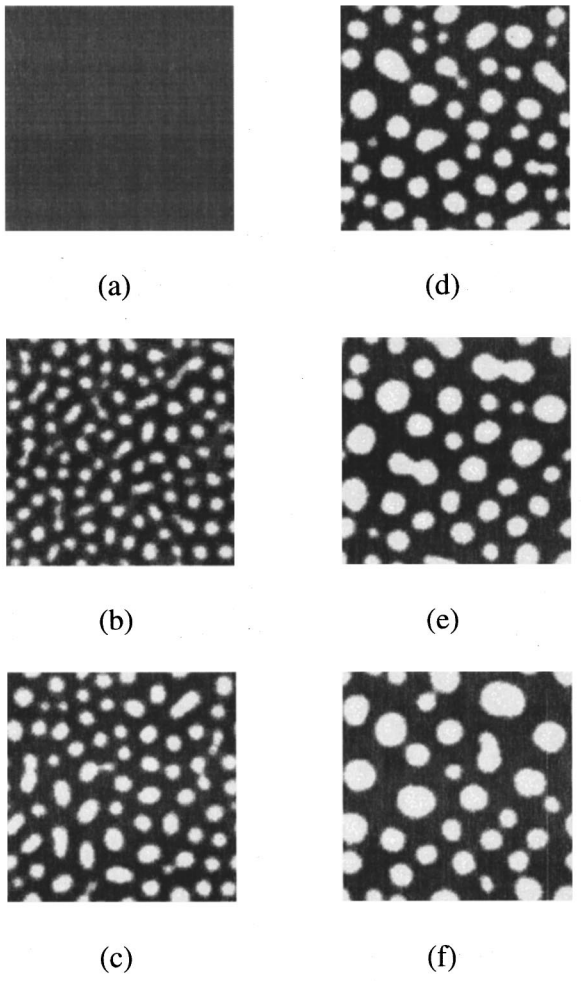

FIG. 5. Snapshots of the pattern at $t=0$ (a), 100 (b), 200 (c), 400 (d), 600 (e), and 800 (f) for $\mathfrak{R}^{-1}=\mathfrak{P}=1.0$ and $\Phi=0.4$. The mass density of A fluid is shown by gray scales.

The inhomogeneity of the order parameter causes the excess stress tensor $\mathbf{\Sigma}^I$, which is expressed as [42,43,13,19]

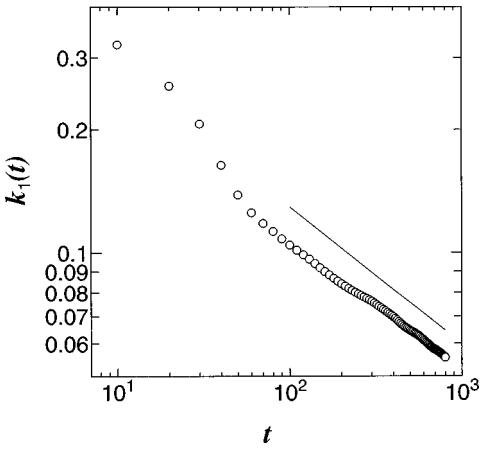

FIG. 6. Double-logarithmic plot of $k_1(t)$ for $\mathfrak{R}^{-1}=\mathfrak{P}=1.0$ and $\Phi=0.4$. The solid line shows the slope $-\frac{1}{3}$.

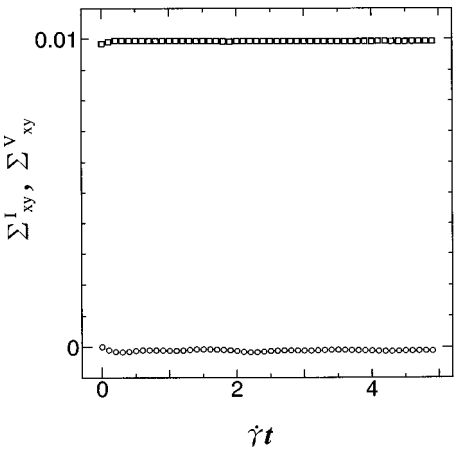

FIG. 7. Time evolution of the shear stress tensors at disordered state ($\epsilon=-0.5,\Phi=0.5$). Σ^I_{xy} and Σ^V_{xy} are plotted by the symbols □ and △, respectively, as functions of shear strain $\dot{\gamma}t$ for $\dot{\gamma}=1.0\times10^{-2}$.

$$\mathbf{\Sigma}^I=-\frac{\hat{K}}{V}\int d\mathbf{r}\nabla S\nabla S \tag{44}$$

$$-\frac{\hat{K}}{V}\sum_\beta \frac{m_\beta}{\rho_\beta}(\nabla S)_\beta(\nabla S)_\beta. \tag{45}$$

We monitor this quantity together with the viscous stress $\mathbf{\Sigma}^V$,

$$\mathbf{\Sigma}^V\simeq\frac{2\mathfrak{R}^{-1}}{V}\sum_\beta \frac{m_\beta}{\rho_\beta}\mathbf{D}_\beta. \tag{46}$$

The total stress tensor is given by the sum of these two stress tensors apart from the isotropic term. The formula Eq. (44) of the stress tensor is well known for binary fluid systems with the Ginzburg-Landau-type free energy. A derivation of the formula in our model is shown in the Appendix.

We first apply the shear flow at the disordered state $\epsilon=-0.5$ and $\Phi=0.5$. We choose the parameters $\mathfrak{R}^{-1}=\mathfrak{P}=1.0$, $p_0=5.0$, $\mathcal{N}=10\,000$, and $\dot{\gamma}=1.0\times10^{-2}$, which is the same order as the characteristic velocity of particles in the simulation without shear. In Fig. 7, Σ^I_{xy} (circles) and Σ^V_{xy} (squares) are plotted as a function of the shear strain $\dot{\gamma}t$, where $\Sigma^I_{\mu\nu}$ and $\Sigma^V_{\mu\nu}$ are $\mu\nu$ components of $\mathbf{\Sigma}^I$ and $\mathbf{\Sigma}^V$, respectively. Σ^I_{xy} is almost zero, and Σ^V_{xy} fluctuates around the steady-state value $\mathfrak{R}^{-1}\dot{\gamma}=1.0\times10^{-2}$ as expected. Indeed the time-averaged value of Σ^V_{xy} for $0\leqslant t\leqslant500$ is $9.93\pm0.01\times10^{-3}$.

Next we impose the shear flow on the systems where the macroscopic domains exist. We let the system grow for 1000 time steps and apply the shear with $\dot{\gamma}=1.0\times10^{-2}$ at $t=0$. Some snapshots are shown in Fig. 8 for $\Phi=0.5$. We also show some snapshots for the off-critical case ($\Phi=0.4$) with $\dot{\gamma}=1.0\times10^{-2}$ in Fig. 9. In this case we apply the shear after 3000 time steps of the initial growth process. It is observed in both cases ($\Phi=0.5$ and 0.4) that the domains are broken and merge in large strain regime ($\dot{\gamma}t>1$) as pointed out by Ohta, Nozaki, and Doi [13]. These topological changes of domains may cause large fluctuations of stress $\mathbf{\Sigma}^I$. We plot

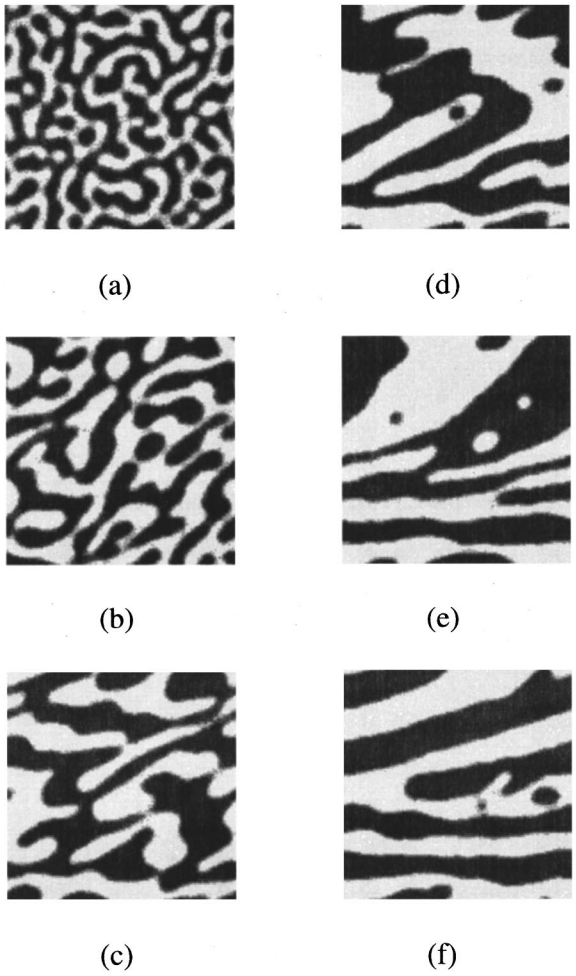

FIG. 8. Snapshots of the system under simple shear flow at $\dot{\gamma}t=0$ (a), 1.0 (b), 2.5 (c), 5.0 (d), 7.5 (e), and 10.0 (f) for $\dot{\gamma}=1.0\times10^{-2}$, $\mathfrak{R}^{-1}=\mathfrak{P}=1.0$, and $\Phi=0.5$.

the shear stress Σ^I_{xy} in Fig. 10 and the normal stress $N_1\equiv\Sigma^I_{xx}-\Sigma^I_{yy}$ in Fig. 11 as functions of shear strain for $\dot{\gamma}=0.01$ (circles), 0.02 (squares), and 0.04 (diamonds), and $\Phi=0.5$. It is difficult to detect the asymptotic steady states in this simulation. In particular, we observe a very slow mode like a relaxational oscillation in Σ^I_{xy} with $\dot{\gamma}=1.0\times10^{-2}$. Such a behavior may be caused by the fact that several parts of domains simultaneously merge or coagulate induced by the flow and form large domains as a result. However, this oscillatory behavior will vanish in the limit of large system size.

IV. SUMMARY AND DISCUSSION

In this paper, we have constructed our numerical model applying the SPH method to the two-fluid model in the absence of elastic force, and demonstrated the simulations for the domain growth kinetics and the rheology under simple shear flow in two dimensions. We have obtained that the dynamic exponent z for the domain growth takes a value close to $\frac{1}{2}$, and that there is a crossover of the exponent from $z=\frac{1}{2}$ to $\frac{2}{3}$ in the low viscosity system. We have confirmed the dynamic scaling for the structure factor in our model sys-

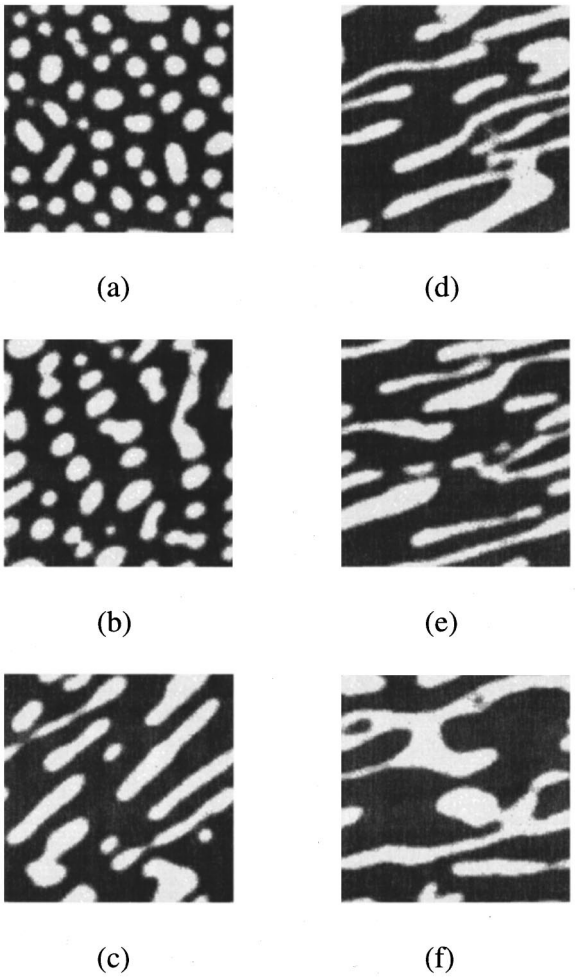

FIG. 9. Snapshots of the system under simple shear flow at $\dot{\gamma}t=0$ (a), 1.0 (b), 2.5 (c), 5.0 (d), 7.5 (e), and 10.0 (f) for $\dot{\gamma}=1.0\times10^{-2}$, $\mathfrak{R}^{-1}=\mathfrak{P}=1.0$, and $\Phi=0.4$.

tems. For simulations under shear flow, we have observed a non-steady-state behavior of the excess stress tensor with large fluctuations caused by topological changes of the domains.

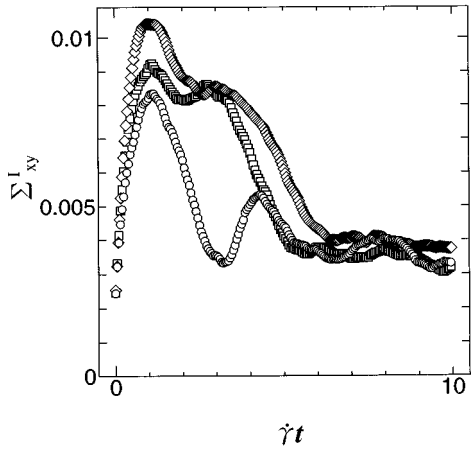

FIG. 10. Time evolution of the shear stress Σ^I_{xy} as functions of $\dot{\gamma}t$ for $\dot{\gamma}=1.0\times10^{-2}$ (circles), 2.0×10^{-2} (squares), and 4.0×10^{-2} (diamonds). $\mathfrak{R}^{-1}=\mathfrak{P}=1.0$ and $\Phi=0.5$.

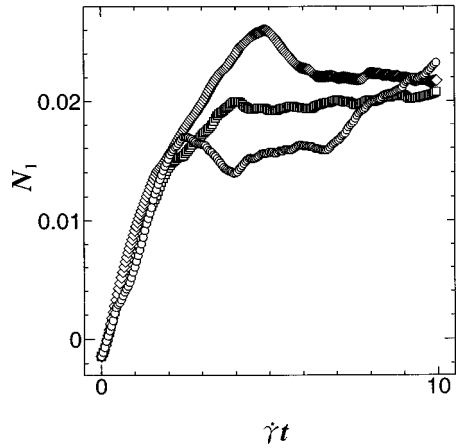

FIG. 11. Time evolution of the normal stress N_1 as functions of $\dot{\gamma}t$ for $\dot{\gamma}=1.0\times10^{-2}$ (circles), 2.0×10^{-2} (squares), and 4.0×10^{-2} (diamonds). $\mathfrak{R}^{-1}=\mathfrak{P}=1.0$ and $\Phi=0.5$.

Our model has the advantage of describing macroscopic phenomena of complex fluids with a reduced number of degrees of freedom compared with the molecular-dynamics method. In addition, we can more easily incorporate external flows into our model than on-lattice models such as the CDS model with hydrodynamic interactions. We believe our model is useful for rheological studies of phase-separating systems, although our model is applicable only to fluid systems.

In the rest of this section, we discuss how to incorporate the effect of the network stress into our model. As mentioned in the preceding sections, for the dynamically asymmetric systems the existence of the network stress $\sigma^{(n)}$ which causes various viscoelastic effects is essential and we cannot neglect the last term in Eq. (2).

Here we consider a system of polymer solution, that is, a polymers (A fluid) plus solvent (B fluid) system, as a special case. In this case the network stress $\sigma^{(n)}$ acts only on the polymers. Indeed the extra force $\mathbf{F}_X$ defined by Eq. (6) becomes $\nabla\cdot\sigma^{(n)}$ or 0 for $X=A$ or B, respectively, in the limit of $N_A\gg N_B$. We can incorporate this extra-force term by replacing σ_{ij} with $\sigma_{ij}+\sigma_i^{(n)}$ in the equation of motion (32) for A particle i, where $\sigma_i^{(n)}$ is the network stress of particle i. In order to complete our model, it must be supplemented by an appropriate constitutive equation which describes time evolution of $\sigma^{(n)}$. One of the simplest model for the constitutive equation is the Maxwell model with a single relaxation time. Such a constitutive equation may be expressed, in terms of our model, as

$$\frac{d}{dt}\sigma_i^{(n)}+\mathbf{\Omega}_i^{(A)}\cdot\sigma_i^{(n)}+(\mathbf{\Omega}_i^{(A)}\cdot\sigma_i^{(n)})^T=-\frac{1}{\tau}\sigma_i^{(n)}+2G_e\mathbf{D}_i^{(A)}, \tag{47}$$

where $\mathbf{\Omega}_i^{(A)}\equiv\frac{1}{2}[(\nabla\mathbf{v}_A)_i-(\nabla\mathbf{v}_A)_i^T]$ is the antisymmetric part of the velocity gradient tensor, or vorticity tensor, for $\mathbf{v}_A$ at $\mathbf{r}_i$, $\mathbf{D}_i^{(A)}$ is the traceless part of symmetric velocity gradient tensor for $\mathbf{v}_A$ at $\mathbf{r}_i$, and τ and G_e are the rheological relaxation time and the elastic shear modulus, respectively, both of which generally depend on ϕ_A. The last two terms in the left-hand side of Eq. (47) come from the rigid body rotation

of the A fluid. It is possible to solve numerically the equations for other constitutive model which may generally include time integrals for the history of each particle. Thus we can directly simulate the dynamics of viscoelastic polymer solutions.

ACKNOWLEDGMENTS

The author would like to thank Professor T. Ohta for valuable discussions and comments. He also thanks Dr. T. Kawakatsu, Dr. A. Ito for fruitful discussions, and Dr. H. Kubotani for providing him with useful information about the SPH method. The computation was partially carried out at Computer Center, University of Tokyo and KEK Computing Center. The author is grateful to Professor M. Furusaka at KEK for his hospitality. This work was supported by a Grant-in-Aid for Encouragement of Young Scientists, from the Ministry of Education, Science and Culture, Japan.

APPENDIX

In this appendix we derive the stress tensor $\mathbf{\Sigma}^I$ [Eq. (44)] due to the inhomogeneity of the order parameter from the equation of motion [Eq. (23)] of particles. Since the order parameter or its conjugate field are even under time reversal, fluctuations of the order parameter contribute to the reversible part of the stress tensor. The dissipative force term in Eq. (23) does not affect $\mathbf{\Sigma}^I$, which is a reversible part of the stress tensor. Therefore, we may start from nondissipative dynamic equations given by

$$m_\alpha \ddot{\mathbf{r}}_\alpha = -\frac{\delta F}{\delta \mathbf{r}_\alpha}, \tag{A1}$$

where F is the total free-energy functional. When F is a functional of the density $\rho(\mathbf{r})$ and the order parameter $S(\mathbf{r})$ which are given by

$$\rho(\mathbf{r}) = \sum_\alpha m_\alpha W(\mathbf{r}-\mathbf{r}_\alpha), \tag{A2}$$

$$S(\mathbf{r}) = [\rho_A(\mathbf{r}) - \rho_B(\mathbf{r})]/\rho(\mathbf{r}) = \sum_\alpha \epsilon_\alpha m_\alpha W(\mathbf{r}-\mathbf{r}_\alpha)/\rho(\mathbf{r}), \tag{A3}$$

where $\epsilon_\alpha = 1$ if particle α is of A type, and $\epsilon_\alpha = -1$ otherwise, and Eq. (A1) is rewritten in the following form:

$$m_\alpha \ddot{\mathbf{r}}_\alpha = -\int d\mathbf{r}\left[\frac{\delta\rho(\mathbf{r})}{\delta \mathbf{r}_\alpha}\frac{\delta F}{\delta\rho(\mathbf{r})} + \frac{\delta S(\mathbf{r})}{\delta \mathbf{r}_\alpha}\frac{\delta F}{\delta S(\mathbf{r})}\right]. \tag{A4}$$

Hereafter we omit the second argument of the smoothing function $W(\mathbf{r}-\mathbf{r}_\alpha, h)$. Substituting Eqs. (A2) and (A3) into Eq. (A4), and integrating by parts, we obtain

$$m_\alpha \ddot{\mathbf{r}}_\alpha = -\int d\mathbf{r}\left[m_\alpha W(\mathbf{r}-\mathbf{r}_\alpha)\nabla\frac{\delta F}{\delta\rho(\mathbf{r})} + \epsilon_\alpha m_\alpha W(\mathbf{r}-\mathbf{r}_\alpha)\nabla\left(\frac{1}{\rho(\mathbf{r})}\frac{\delta F}{\delta S(\mathbf{r})}\right)\right]. \tag{A5}$$

Now consider the total force acting on the system $\int d\mathbf{r}(\partial/\partial t)(\rho\mathbf{v})$, where $\rho\mathbf{v}$ is the momentum density. In our model,

$$\rho\mathbf{v} = \sum_\alpha m_\alpha \dot{\mathbf{r}}_\alpha W(\mathbf{r}-\mathbf{r}_\alpha). \tag{A6}$$

Hence

$$\int d\mathbf{r}\frac{\partial}{\partial t}(\rho\mathbf{v}) = \sum_\alpha \int d\mathbf{r} m_\alpha [\ddot{\mathbf{r}}_\alpha W(\mathbf{r}-\mathbf{r}_\alpha) - \dot{\mathbf{r}}_\alpha\dot{\mathbf{r}}_\alpha\cdot\nabla W(\mathbf{r}-\mathbf{r}_\alpha)]. \tag{A7}$$

From Eqs. (A2), (A3), (A5), and (A7) we obtain

$$\int d\mathbf{r}\left[\frac{\partial}{\partial t}(\rho\mathbf{v}) + \nabla\cdot(\rho\mathbf{v}\mathbf{v})\right] = -\int d\mathbf{r}\left[\rho(\mathbf{r})\nabla\frac{\delta F}{\delta\rho(\mathbf{r})} + [\rho_A(\mathbf{r}) - \rho_B(\mathbf{r})]\nabla \times\left(\frac{1}{\rho(\mathbf{r})}\frac{\delta F}{\delta S(\mathbf{r})}\right)\right]. \tag{A8}$$

Here we have used the property $\int d\mathbf{r} W(\mathbf{r}-\mathbf{r}_\alpha) = 1$ and $\rho\mathbf{v}\mathbf{v} \equiv \Sigma_\alpha m_\alpha \dot{\mathbf{r}}_\alpha \dot{\mathbf{r}}_\alpha W(\mathbf{r}-\mathbf{r}_\alpha)$.

If we assume the incompressibility, that is, $\nabla\rho(\mathbf{r}) = \mathbf{0}$, Eq. (A8) becomes

$$\int d\mathbf{r}\left[\frac{\partial}{\partial t}(\rho\mathbf{v}) + \nabla\cdot(\rho\mathbf{v}\mathbf{v})\right] = -\int d\mathbf{r}[\nabla p + S\nabla\mu], \tag{A9}$$

where $p \equiv \rho(\delta F/\delta\rho)$ is the pressure and $\mu \equiv \delta F/\delta S$ is the chemical potential. The last term in Eq. (A9) gives rise to the excess stress tensor. When the chemical potential is derived from Ginzburg-Landau-type free energy and can be written in the form, $\mu = (\partial f/\partial S) - K\nabla^2 S$, with some known function $f(S)$, the last term in Eq. (A9) can be written as

$$S\nabla\mu = \nabla\left(S\frac{\partial f}{\partial S} - f - KS\nabla^2 S - \frac{K}{2}|\nabla S|^2\right) + K\nabla\cdot(\nabla S\nabla S). \tag{A10}$$

The first term on the right-hand side of Eq. (A10) only contributes to the isotropic term of the stress tensor, which is not of interest in incompressible flow and can be included in the pressure term. Equations (A9) and (A10) imply that the excess stress tensor is given by $-K\nabla S\nabla S$ apart from the isotropic term. Therefore, we obtain the stress tensor for the whole the system

$$\mathbf{\Sigma}^I = -\frac{K}{V}\int d\mathbf{r}\nabla S\nabla S, \tag{A11}$$

where V is the total volume of the system.

[1] T. Hashimoto, Phase Transit. **12**, 47 (1988).
[2] J. D. Gunton, M. San Miguel, and P. S. Sahni, in *Phase Transitions and Critical Phenomena*, edited by C. Domb and J. L. Lebowitz (Academic, New York, 1983), Vol. 8.
[3] T. Koga and K. Kawasaki, Physica A **196**, 389 (1993), and references therein.
[4] A. Shinozaki and Y. Oono, Phys. Rev. E **48**, 2622 (1993), and references therein.
[5] D. H. Rothman, Rev. Mod. Phys. **66**, 1417 (1994), and references therein.
[6] P. C. Hohenberg and B. I. Halperin, Rev. Mod. Phys. **49**, 435 (1977).
[7] Y. Oono and S. Puri, Phys. Rev. A **38**, 434 (1988).
[8] S. Puri and Y. Oono, Phys. Rev. A **38**, 1542 (1988).
[9] W. J. Ma, A. Maritan, J. R. Banavar, and J. Koplik, Phys. Rev. A **45**, R5347 (1992).
[10] E. Velasco and S. Tuxvaerd, Phys. Rev. Lett. **71**, 388 (1993).
[11] M. Doi and A. Onuki, J. Phys. II **2**, 1631 (1992).
[12] J. J. Monaghan, Annu. Rev. Astron. Astrophys. **30**, 543 (1992), and references therein.
[13] T. Ohta, H. Nozaki, and M. Doi, Phys. Lett. A **145**, 304 (1990); J. Chem. Phys. **93**, 2664 (1990).
[14] M. Doi and T. Ohta, J. Chem. Phys. **85**, 1242 (1991).
[15] J. F. Olson and D. H. Rothman, J. Stat. Phys. **81**, 199 (1995).
[16] H. Tanaka, Phys. Rev. Lett. **71**, 3158 (1993); J. Chem. Phys. **100**, 5323 (1994); Phys. Rev. Lett. **76**, 787 (1996).
[17] F. Brochard and P. G. de Gennes, Macromolecules **10**, 1157 (1977).
[18] P. G. de Gennes, *Scaling Concepts in Polymer Physics* (Cornell University Press, Ithaca, NY, 1979).
[19] M. Doi, in *Dynamics and Patterns in Complex Fluids*, edited by A. Onuki and K. Kawasaki (Springer, Berlin, 1990).
[20] A. Onuki, J. Phys. Soc. Jpn. **59**, 3423 (1990); **59**, 3427 (1990).
[21] S. T. Milner, Phys. Rev. Lett. **66**, 1477 (1991).
[22] W. G. Hoover, T. G. Pierce, C. G. Hoover, J. O. Shugart, C. M. Stein, and A. L. Edwards, Comput. Math. Appl. **28**, 155 (1994).
[23] H. A. Posch, W. G. Hoover, and O. Kum, Phys. Rev. E **52**, 1711 (1995).
[24] X. F. Yuan, R. C. Ball, and S. F. Edwards, J. Non-Newtonian Fluid Mech. **46**, 331 (1993); **54**, 423 (1994).
[25] N. A. Spenley, X. F. Yuan, and M. E. Cates, J. Phys. II **6**, 551 (1996).
[26] M. Doi and S. F. Edwards, *The Theory of Polymer Dynamics* (Clarendon, Oxford, 1986).
[27] E. D. Siggia, Phys. Rev. A **20**, 595 (1979).
[28] K. Kawasaki and T. Ohta, Physica A **118**, 175 (1983).
[29] J. E. Farrell and O. T. Valls, Phys. Rev. B **42**, 2353 (1990).
[30] H. Furukawa, Adv. Phys. **34**, 703 (1985), and references therein.
[31] H. Furukawa, Physica A **204**, 237 (1994).
[32] C. Appert, J. F. Olson, D. H. Rothman, and S. Zaleski, J. Stat. Phys. **81**, 181 (1995).
[33] A. Shinozaki and Y. Oono, Phys. Rev. Lett. **66**, 173 (1991).
[34] C. Yeung, Phys. Rev. Lett. **61**, 1135 (1988).
[35] H. Furukawa, J. Phys. Soc. Jpn. **58**, 216 (1989).
[36] T. Ohta and H. Nozaki, in *Space-Time Organization in Macromolecular Fluids*, edited by F. Tanaka, M. Doi, and T. Ohta (Springer, Berlin, 1989).
[37] G. Porod, in *Small Angle X-Ray Scattering*, edited by O. Glatter and O. Kratky (Academic, New York, 1982).
[38] F. S. Bates and P. Wiltzius, J. Chem. Phys. **90**, 3258 (1989).
[39] M. Takenaka and T. Hashimoto, J. Chem. Phys. **96**, 6177 (1992).
[40] K. Kubota, N. Kuwahara, H. Eda, M. Sakazume, and K. Takiwaki, J. Chem. Phys. **97**, 9291 (1992).
[41] M. P. Allen and D. J. Tildesley, *Computer Simulation of Liquids* (Clarendon, Oxford, 1987).
[42] K. Kawasaki, Phys. Rev. **150**, 291 (1966).
[43] A. Onuki, Phys. Rev. A **35**, 5149 (1987).